IOP Conference Series: Materials Science and Engineering

1D N-type SnO_2 nanofibers coexisted with P-type Co_3O_4 cubes for highly selective acetone sensor

1D N-type SnO_2 nanofibers coexisted with P-type Co_3O_4 cubes for highly selective acetone sensor

W Tang[1], D W Li, X J Du, J Yu and Q Q Sun

Shandong Province Key Laboratory of Medical Physics and Image Processing Technology, School of Physics and Electronics, Shandong Normal University, Jinan 250014, Jinan Province, China

[1] E-mail: tangweiyouxiang@foxmail.com

Abstract. 1D n-type SnO_2 nanofibers coexisted with p-type Co_3O_4 particles were synthesized by electrospinning with subsequent hydro-thermal process. The morphology and composition of Co_3O_4/SnO_2 were characterized by X-ray diffraction (XRD), scanning electron microscope (SEM). XRD patterns showed that the synthesized Co_3O_4/SnO_2 were assigned to cubic Co_3O_4 and tetragonal rutile structure of SnO_2 without any other impurity peaks. A possible growth mechanism was proposed to describe the formation of hierarchical SnO_2 nanofibers coexisted with Co_3O_4 cubes. The Co_3O_4/SnO_2 compound exhibited a relatively highly selective response to acetone and stable acetone sensing performance after a long period of aging. The Co_3O_4/SnO_2 compound had a p-type response. It may be ascribed to the high coverage of p-type Co_3O_4 on n-type SnO_2. The excellent acetone sensing properties of Co_3O_4/SnO_2 nanostructures may be attributed to p-n junctions between Co_3O_4 and SnO_2 nanograins as well as the unique coexistence structure of nanofibers and cubes.

1. Introduction

Acetone as a widely used industrial raw material is regarded as a huge threat to human's health especially exposure to high concentration over 100000 ppm. It is reported that the acetone concentration in exhaled breath of diabetic patients is much higher than healthy people [1]. Therefore, in consideration of health and safety, there is a huge demand for detecting acetone concentration in public or human body.

Currently, a lot of metal oxide semiconductors (MOS) have been applied to detect harmful and toxic gases. These sensors based on MOS have many advantages such as high sensitivity, short respond/recovery time and simple synthesis route, but they also have disadvantages of poor selectivity, high operating temperature and low sensitivity to ultra-low concentrations of gases [2]. Several strategies including the use of compound metal oxides [3, 4], heterostructure formation [5, 6], transition metal catalyst doping [7, 8] and UV light irradiation [9] have been used to overcome these drawbacks. For example, surface modification with noble metal (Au, Pd, Ag) nanopaoticles as sensitizer is the most common approach to improve the gas sensing properties due to the catalytic overflow effect of noble metal particles. Meanwhile, the p-n heterojunction method is also an effective strategy to improve gas sensitive parameters of SnO_2-based gas sensors. P-n heterostructures can be obtained by mixing compound structures, forming core-shell structures, decorating with second-phase particles and building bi-layer or multi-layer films [10].

P-type Co_3O_4 with a direct band gap of about 2 eV, is one of most interesting materials with huge potential applications such as lithium-ion batteries [11], VOC gas sensors [12], catalyst [13], electrochemistry [14], supercapacitor [15]. So far various methods have been developed to synthesize Co_3O_4 with different nanostructures such as nanocubes [16], nanosheets [17, 18], and nanofibers [19]. It is considered as an excellent active material loaded on a host oxide due to its good conductivity, high catalytic reactivity, stable chemical activity [20], and its special structure which facilitates electron transportation between Co^{2+} and Co^{3+} ions. However, in the field of gas sensors, a serious shortcoming of low sensitivity has limited the application of Co_3O_4 in actual implementation. Up to now, numerous modification methods have been adopted to improve the gas sensing characteristics of Co_3O_4 as a high sensitive material at low operating temperature. Among them, compositing with n-type semiconductor is a good choice because it not only strengthens the interactions of closely packed nano-units but also extends the electron depletion layer by forming p-n heterojunctions [21, 22]. As is known to all, SnO_2 is a typical n-type semiconductor with excellent gas sensing properties except the poor selectivity.

In this study, n-SnO_2 NFs coexisted with p-type Co_3O_4 cubic nanoparticles were synthesized by electrospinning with subsequent hydrothermal process. The acetone gas sensing properties were tested. In particular, the origin of the enhanced acetone response of Co_3O_4/SnO_2 compared to pure Co_3O_4 is discussed from the perspective of p-n heterojunctions [23].

2. Experimental details

2.1. Synthesis of material

Synthesis of SnO_2 nanofibers. SnO_2 NFs were synthesized by simple electrospinning that our group reported before [24]. Briefly, 1 mmol of $SnCl_2 \cdot 2H_2O$ were dissolved in 4.2 mL of EtOH solvent at room temperature with magnetic stirring for 30 minutes. Subsequently, a certain amount of PVP and 3.5 mL of DMF were added into above solution, agitating for 8 h. The relevant parameters were as follows: the voltage and the distance between the needle (positive pole) and the collector (negative pole) were 18 kV and 15 cm, respectively. The diameter of the needle was 0.7 mm.

Synthesis of Co_3O_4 cubic nanoparticles. $Co(NO_3)_2 \cdot 6H_2O$, CTAB, methanol were of analytical grade, without further purification. 4 g $Co(NO_3)_2 \cdot 6H_2O$ and 2 g CTAB were dissolved in 12 mL deionized water and 60 mL methanol, sonication for 30 min. The solution was transferred to 100 mL Teflon autoclaves and heated at 180 for 24 h. The products were obtained by centrifugation and annealed at 600°C for 3 h.

Synthesis of Co_3O_4/SnO_2 heterostructures. 0.05 g SnO_2 NFs with annealed at 600°C for 3 h were added into the Co_3O_4 hydrothermal solution. Hydrothermal reaction process is the same as the second step.

2.2. Fabrication and measurement of gas sensors

The fabrication and gas sensing test of the sensors were the same as our group reported before [22], as shown in Figure 1. The sintered samples were mixed with a suitable amount of deionized water and then grinded for 30 min to form a paste. The paste was coated on a clean ceramic tube with a pair of gold test electrodes. After that the ceramic tubes were sintered at 500°C for 3 h in air. Subsequently, a Ni-Cr heating wire was inserted into the tube to fabricate a side-heating gas sensor. Before testing gas sensing properties, the fabricated sensors should be aged at 300°C for 7 days in air to improve device stability. The gas sensing properties were measured in a range of 100°C~200°C in a home-built static test system. The response of n-type sensor was defined as S=Ra/Rg while p-type sensor is the opposite, of which Ra and Rg referring to the stable resistance values in air and in target gas, respectively.

2.3. Characterizations

The Co_3O_4/SnO_2 heterostructures were analyzed by XRD (Shimadzu XRD-6000, Japan) in 2θ region of 20-80° with Cu Kα 1 (0.15406 nm) radiation. Scanning electron microscopy (SEM) was carried out

on a FEI QUANTA 200F (USA) microscope equipped with energy-dispersive X-ray (EDX) spectroscopy.

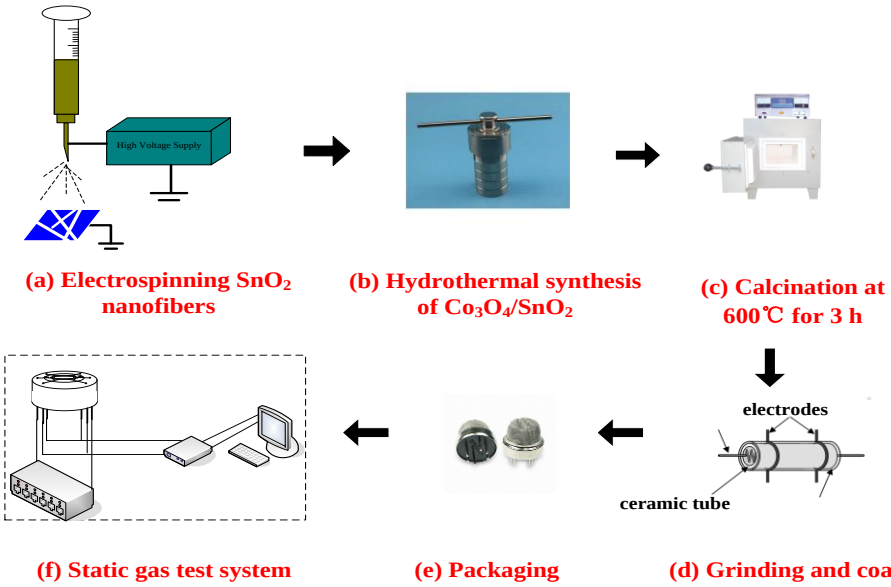

Figure 1. Schematic of synthesis, fabrication and sensing test of Co_3O_4/SnO_2 based sensors.

3. Results and discussion

3.1. X-ray diffraction (XRD)

Figure 2 presents the XRD patterns of Co_3O_4 and Co_3O_4/SnO_2. All the peaks of Co_3O_4 were assigned to cubic cobalt oxide with lattice constants of a=b=c=8.118 Å (PDF#80-1534). All the diffraction peaks of pure SnO_2 can be indexed to pure tetragonal rutile structure of SnO_2 (PDF#77-0452). In the XRD pattern of Co_3O_4/SnO_2, in addition to the reflections from Co_3O_4, peaks from (110), (101), (211), (220) and (321) lattice planes of SnO_2 with lattice constants of a= 4.755 Å were identified. No diffraction peaks from any other impurities were observed. The continuous diffraction peaks indicates that the synthesized samples become essentially amorphous after high temperature calcination.

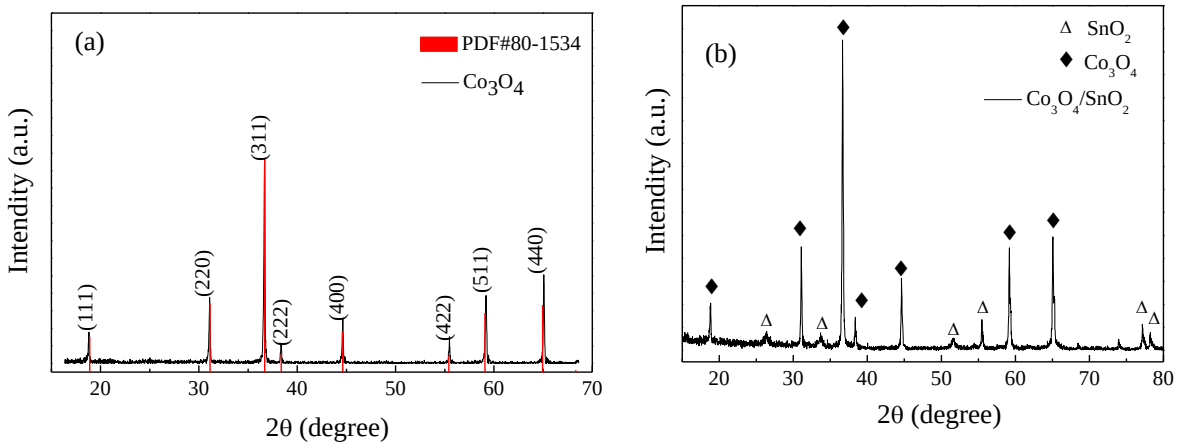

Figure 2. XRD patterns of Co_3O_4 and Co_3O_4/SnO_2.

3.2. Scanning electron microscopy (SEM)

The morphology of Co_3O_4, Co_3O_4/SnO_2 and SnO_2 were investigated by SEM characterization. From Figure 3(a) and (b) it can be seen that Co_3O_4 have a clearly cube structure. The observed six planes of nanocubes are bound by planes of Co_3O_4 crystal with spinel structure [16]. However, when loading Co_3O_4 cubic nanoparticles with SnO_2 nanofibers, cubic Co_3O_4 decomposed into blocks. Meanwhile Co_3O_4/SnO_2 exhibited a special morphology of coexistence of blocks and fibers, of which fibers are SnO_2 and blocks are Co_3O_4, as shown in Figure 3(c). Figure 3(d) shows that the SnO_2 nanofibers prepared by electrospinning is one dimensional and has hollow hierarchical structure. It further indicates that the introduction of different metal oxide with opposite conductive type has a great influence on the morphology of the main materials.

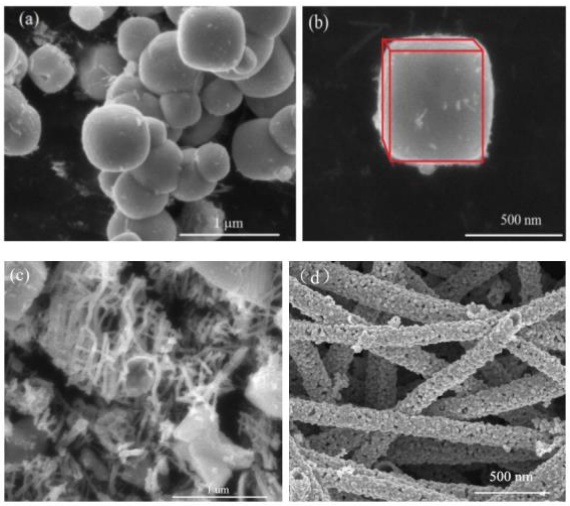

Figure 3. SEM images of (a) Co_3O_4 cubes, (b) individual Co_3O_4 cube, (c) Co_3O_4/SnO_2 compound and (d) SnO_2.

3.3. Growth process and acetone sensing properties

Figure 4 is the schematic illustration for possible formation processes of SnO_2 nanofibers, cubic Co_3O_4 and Co_3O_4/SnO_2. For SnO_2 nanofibers, Sn^{2+}, Cl^-, NO_3^- and PVP chain are evenly mixed to form compound nanofibers in the electrospinning period. When heating treatment, the anions are decomposed by oxidation while the cations are oxidized and crystallized into small particles, agglomerate into big ones and connect together to form nanofibers eventually. With post-heat treatment, the unstable Co_3O_4 precursor recrystallized into Co_3O_4 with a stable cube structure. For Co_3O_4/SnO_2 structures, the as synthesized SnO_2 nanofibers were added into the Co_3O_4 hydrothermal solution to mix uniformly. During the hydrothermal reaction process with high temperature and high pressure, the Co_3O_4 precursor and SnO_2 recrystallized to form heterojunction structure.

Figure 5 indicates the responses of the Co_3O_4 and Co_3O_4/SnO_2 gas sensors as a function of operating temperature in a range of 100~ 200°C and the acetone concentration is 10 ppm. The sensitivities of Co_3O_4 and Co_3O_4/SnO_2 gas sensors were highest at 150°C. Therefore, 150°C was chosen as optimal operating temperatures for both Co_3O_4 and Co_3O_4/SnO_2 gas sensors in the following gas sensing measurement. The maximum responses of the sensors at 150°C may be ascribed to the different activation energies of pre-adsorbed surface oxygen species at different temperatures.

Figure 6(a) and (b) show the sensitivities of gas sensors based on Co_3O_4 and Co_3O_4/SnO_2 to different acetone concentrations in a range of 1~75 ppm at operating temperature of 150°C, respectively. It can be seen that the response of the gas sensor based on Co_3O_4/SnO_2 compound is much higher than that of gas sensor based on Co_3O_4 cubic nanoparticles. Once upon exposure to acetone, the resistances of the two sensors increase rapidly, exhibiting typical p-type conductivity. However, the resistances of both sensors could return to initial resistance level upon removing acetone.

Meanwhile, for different cycles of injecting-releasing acetone, both sensors can recover to their initial states, indicating a good reproducibility of Co_3O_4 and Co_3O_4/SnO_2 sensors. With the increasing of acetone concentration, the sensor based on Co_3O_4/SnO_2 presents good response to acetone, showing a relatively good linear response-concentration relationship while the response values of Co_3O_4 increase exponentially with acetone concentration, showing nonlinear response characteristics. Figure 7 is the response/recovery curve of Co_3O_4/SnO_2 based sensors to 20 ppm acetone. According to the definition of response time and recovery time, the response/recovery time of Co_3O_4/SnO_2 based sensors are 44 s and 23 s respectively.

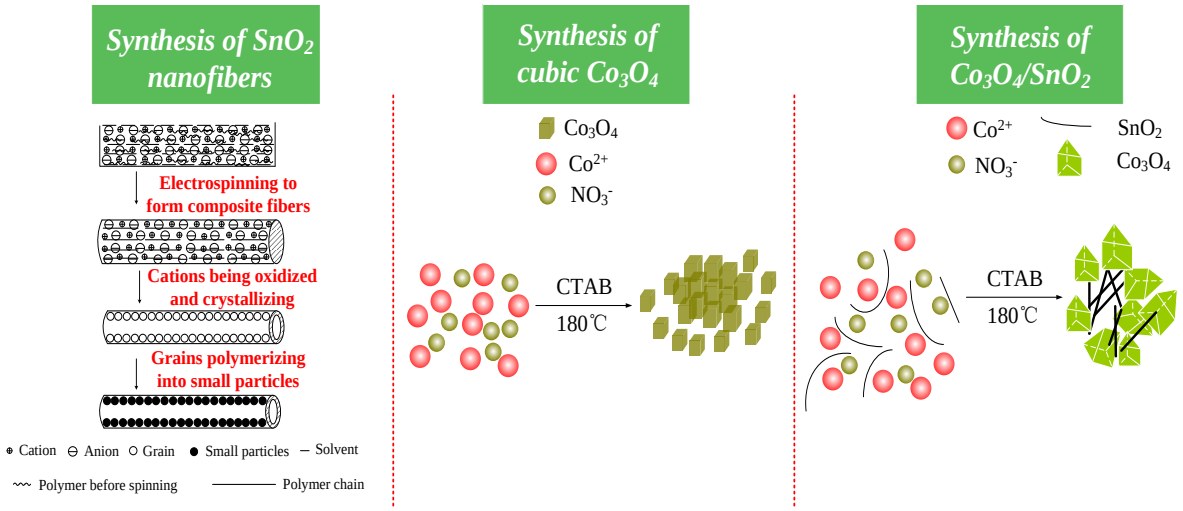

Figure 4. Schematic illustration for possible formation processes of SnO_2 nanofibers, cubic Co_3O_4 and Co_3O_4/SnO_2.

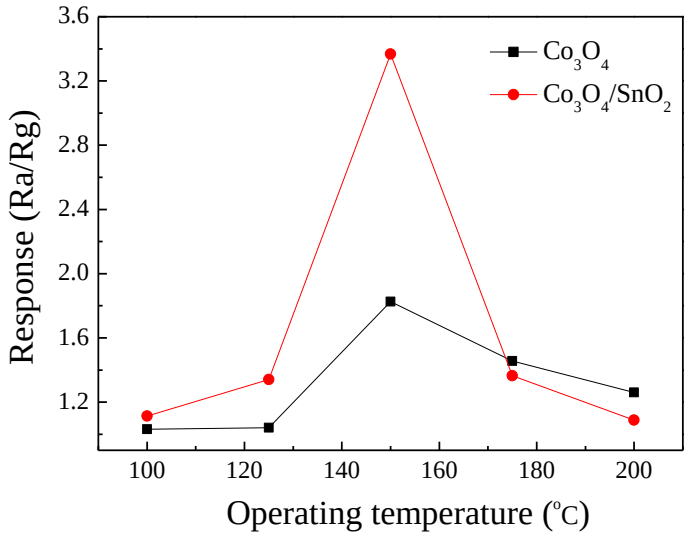

Figure 5. Responses of Co_3O_4 and Co_3O_4/SnO_2 gas sensors vs operating temperatures.

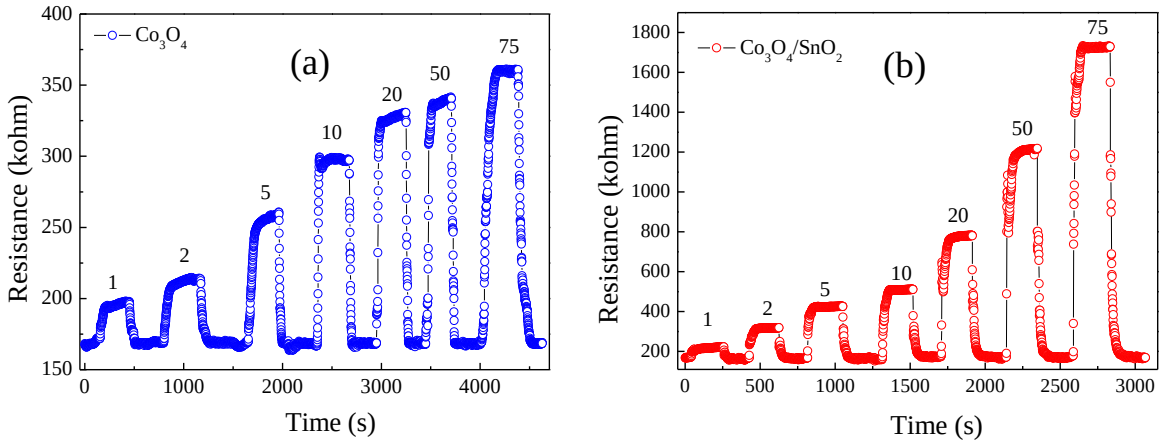

Figure 6. Dynamic response curves of (a) Co_3O_4 cubes, (b) Co_3O_4/SnO_2 to acetone in a range of 1-75 ppm.

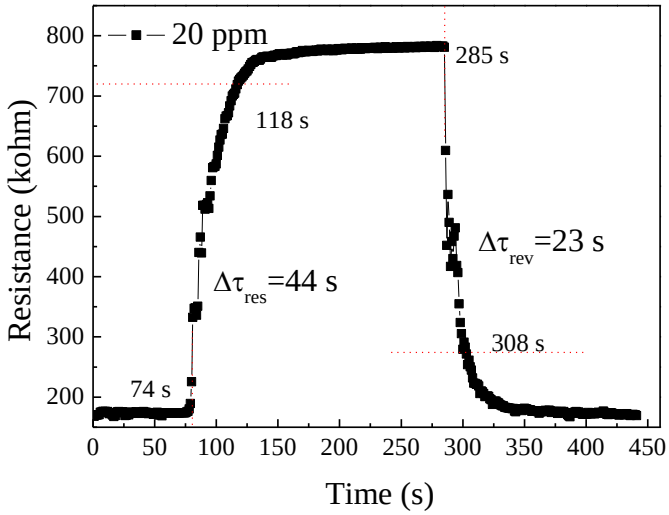

Figure 7. Response/recovery curves of Co_3O_4/SnO_2 based sensors to 20 ppm acetone.

Selectivity is an important gas sensing parameter for practical gas sensors. The improvement of selectivity mainly depends on the development of new sensitive materials and the use of catalysts. In this work, the sensitivity of Co_3O_4 based sensors is improved by the introducing of SnO_2. The responses of Co_3O_4 and Co_3O_4/SnO_2 gas sensors to five interference gases including formaldehyde, ethanol, toluene, methanol and ammonia with a concentration range of 10 ppm were examined, as shown in Figure 8. The response of the Co_3O_4/SnO_2 gas sensor to acetone is higher than the sensitivities to the other interference gases. Therefore, it can be concluded that the Co_3O_4/SnO_2 gas sensor has a good selectivity to acetone. Meanwhile, the selectivity of Co_3O_4/SnO_2 is better than that of Co_3O_4.

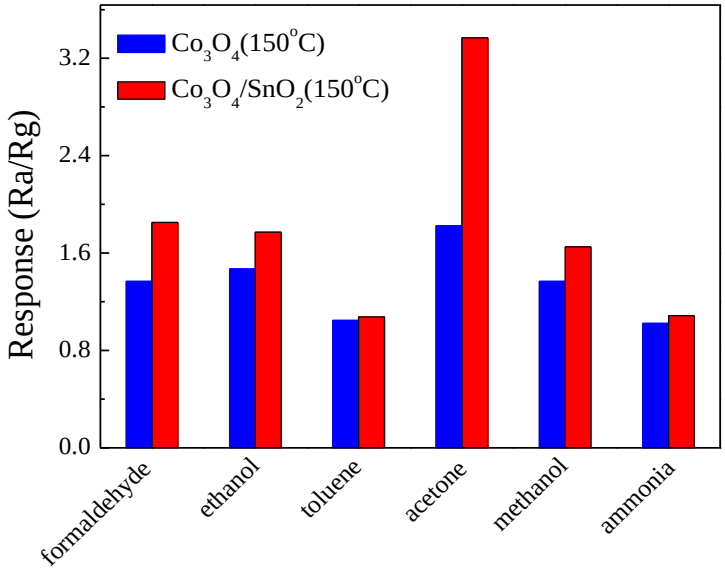

Figure 8. Responses of Co_3O_4 and Co_3O_4/SnO_2 gas sensors to different gases.

Figure 9 gives the long-term stabilities of Co_3O_4 and Co_3O_4/SnO_2 gas sensors in 10 ppm acetone vapor with a measurement temperature range of 10~15°C. From the curves we can see that the response of Co_3O_4/SnO_2 based sensors has picked up after four weeks' aging while the response of Co_3O_4 continues to decrease. On the whole, the responses of Co_3O_4/SnO_2 based sensors do not change very much in this time range, indicating a good stability of the fabricated sensors.

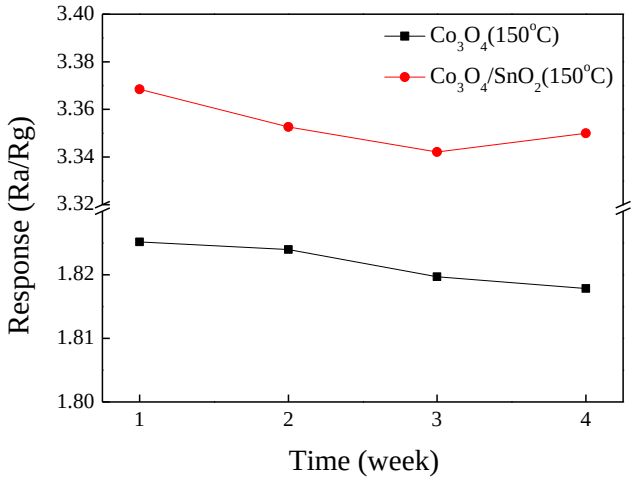

Figure 9. Long-term stabilities of Co_3O_4 and Co_3O_4/SnO_2 based sensors to 10 ppm acetone over 4 weeks.

In addition, the sensing properties of our fabricated Co_3O_4/SnO_2 gas sensors are compared with other published Co_3O_4/SnO_2 gas sensors, as shown in Table 1. It can be seen that the sensing properties of our fabricated Co_3O_4/SnO_2 gas sensors are comparable to those of the previously reported Co_3O_4/SnO_2 sensors. For example, the optimal working temperature of our fabricated Co_3O_4/SnO_2 gas sensors is lower than Co_3O_4-decorated SnO_2 nanowires [25], Co_3O_4/SnO_2 compound [26] and Co_3O_4-loaded SnO_2 thick films [27]. According to different microstructures, components and synthesis methods, the gas sensing response of Co_3O_4/SnO_2 based sensors can be either p-type or n-type. However, most of the test gas species of the reported Co_3O_4/SnO_2 based sensors are oxidized gases

and hydrogen, few VOC gases were measured. The higher response of [28] and [29] may be attributed to the difference relative molecular mass of gases. It has been reported that smaller molecules can interact and diffuse more efficiently on the surface of sensitive materials than others with greater molecular mass [30]. Even though certain sensing parameters of our fabricated Co_3O_4/SnO_2 based sensors are not as good as the previously reported, the gas sensing abilities of the synthesized Co_3O_4/SnO_2 can be improved by optimizing grain size through modulating the temperature and time of hydrothermal reaction and calcination in the future work.

3.4. Sensing Mechanism

As known to all, the pre adsorbed oxygens in air play an important role in the gas sensing reaction. In an air environment at the optimum operating temperature, the oxygen molecules will be adsorbed on the surface of the semiconductor metal oxides and extract electrons to form adsorbed oxygen species such as O_2^-, O^- and O^{2-}. At the same time, a depletion layer and junctions are formed at the grain boundaries.

For Co_3O_4/SnO_2, lots of Co_3O_4/SnO_2 heterojunctions are simultaneously generated in addition to the SnO_2/SnO_2 homojunctions, as shown in Figure 10. When n-type SnO_2 and p-type Co_3O_4 nanograins come into contact, electrons will flow from n-type SnO_2 to p-type Co_3O_4 until the Fermi level on each side reached an equilibrium, forming an hole depletion layer on the Co_3O_4 side and an electron depletion layer on the SnO_2 side. As a result, the resistances of Co_3O_4/SnO_2 increased greatly. Upon exposure to acetone, as both SnO_2 and Co_3O_4 have reactivity to acetone, the electrons are given back to the conduction bands of SnO_2 and Co_3O_4. It results in the decrease of band bending in SnO_2. However, because Co_3O_4 is almost inactive to acetone, the conduction band of Co_3O_4 remained almost unchanged. Therefore the height of potential barriers in Co_3O_4/SnO_2 increased. In this way, the resistance of Co_3O_4/SnO_2 sensors towards acetone increased and showed a p-type response. The additional resistance change of Co_3O_4/SnO_2 is the main factor of enhanced gas sensing properties of Co_3O_4/SnO_2.

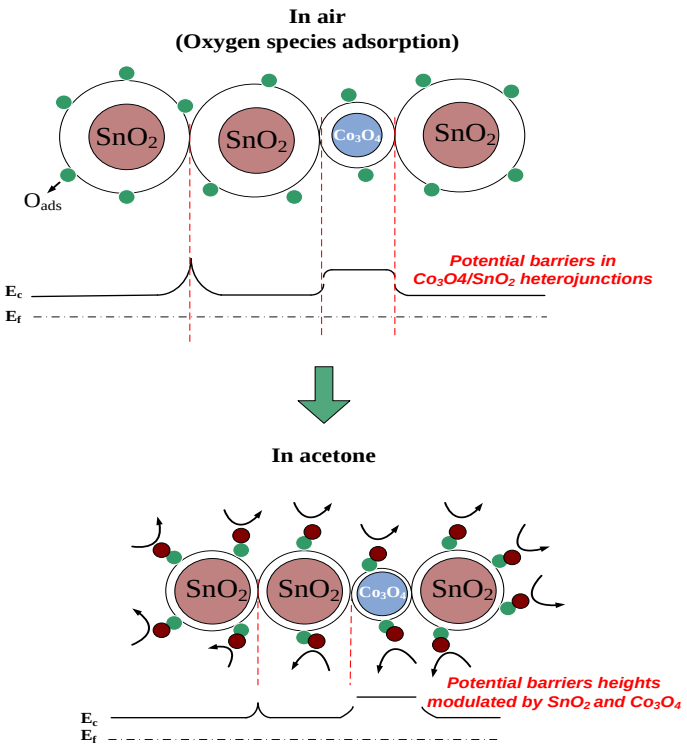

Figure 10. The possible sensing mechanism model for Co_3O_4/SnO_2-based sensors.

Table 1. Comparison of sensing properties of our Co_3O_4/SnO_2 sensors with previously reported Co_3O_4/SnO_2 sensors.

Structures	Gas species	Concentration (ppm)	Operating temperature (^oC)	Response & conductive type	Reference
Co_3O_4-decorated SnO_2 nanowires	NO_2	2-10	300	3.5/10 ppm p-type	[25]
Co_3O_4/SnO_2 composites	H_2	5-200	300	-- p-type	[26]
Co_3O_4/SnO_2 system	CO	20-1000	25	192/1000 ppm p-type	[28]
Co_3O_4/SnO_2 thick films	CO	10	250	100 n-type	[29]
Co_3O_4-loaded SnO_2 thick films	alcohol	1000	300	301 n-type	[27]
SnO_2 nanofibers loaded with p-type Co_3O_4 cubic	acetone	10	150	3.7 p-type	this work

4. Conclusions

To put it generally, n-SnO_2 nanofibers coexisted with p-Co_3O_4 cubes were synthesized by electrospinning with subsequent hydrothermal process, and their acetone sensing properties were tested. The Co_3O_4/SnO_2 exhibited a relatively highly selective response to acetone and stable sensing performance. Meanwhile, the sensing response of the Co_3O_4/SnO_2 manifested as Co_3O_4 do, namely p-type response. It may be ascribed to the high coverage of p-type Co_3O_4 on n-type SnO_2. The origin of the enhanced acetone response of Co_3O_4/SnO_2 is attributed to p-n heterojunctions between Co_3O_4 and SnO_2 nanograins as well as the unique structure of coexistence of Co_3O_4 cubics and SnO_2 nanofibers. This work may be helpful for clarifying the gas sensing mechanism in p-n heterojunctions.

Acknowledgements

This work was supported by National Natural Science Foundation of China (61801276), Shandong Province Natural Science Foundation (ZR2018BF003) and Youth Science and Technology Cultivation Fund of Shandong Normal University.

Conflicts of Interest: The author declare no conflict of interest.

References

[1] Righettoni M, Tricoli A 2011 *J. Breath Res.* **5** 037109
[2] Park S, Sun G J, Kheel H, Lee W I, Lee S, Choi S B, Lee C 2016 *Sens. Actuators B* **227** 591
[3] Zhang J, Liu X H, Wang L W, Yang T L, Guo X Z, Wu S H, Wang S R, Zhang S M 2011 *Nanotechnology* **22** 185501
[4] Na C W, Woo H S, Kim I D, Lee J H 2011 *Chem. Commun.* **47** 5148
[5] Wang L, Deng J, Lou Z, Zhang T 2014 *J. Mater. Chem. A* **2** 10022
[6] Park S, Park S, Jung J, Hong T, Lee S, Kim H W, Lee C 2014 *Ceram. Int.* **40** 11051
[7] Kim H, Jin C, Park S, Kim S, Lee C 2012 *Sens. Actuators B* **161** 594
[8] Wan Q, Wang T H 2005 *Chem. Commun.* **30** 3841

[9] Fan S W, Srivastava A K, Dravid V P 2009 *Appl. Phys. Lett.* **95** 142106.
[10] Miller D R, Akbar S A, Morris P A 2014 *Sens. Actuators B* **204** 250
[11] Li W Y, Xu L N, Chen J 2005 *Adv. Funct. Mater.* **15** 851
[12] Nguyen H, Elsafty S A 2011 *J. Phys. Chem. C* **115** 8466
[13] Lee H T, Kwon S, Youn C M, Choi T, Lee J H 2017 *Eur. J. Inorg. Chem.* **2017** 2184
[14] Jamil S, Khan S R 2017 *Aust. J. Chem.* **70**
[15] You Y, Zheng M, Ma L, Yuan X, Zhang B, Li Q, Wang F, Song J, Jiang D, Liu P 2017 *Nanotechnology* **28** 105604
[16] Zhou T, Zhang T, Deng J, Zhang R, Lou Z, Wang L 2017 *Sens. Actuators B* **242** 369
[17] Lin Y, Ji H, Shen Z, Jia Q, Wang D 2016 *J. Mater. Sci.-Mater. Electron.* **27** 2086
[18] Deng S, Liu X, Chen N, Deng D, Xiao X, Wang Y 2016 *Sens. Actuators B* **233** 615
[19] Shao C L, Guan H Y, Wen S B, Chen B, Yang X H, Gong J, Liu Y C 2004 *Chin. Chem. Lett.* **15** 492
[20] Wang X, Tian W, Zhai T, Zhi C, Bando Y, Golberg D 2012 *J. Mater. Chem* **22** 23310
[21] Jiang P, Zhang H, Chen C M, Liang J J, Luo Y, Zhang M, Cai M Q 2017 *Crystengcomm* **19(38)**, 5742
[22] Wang L, Zheng L, Rui Z, Zhou T T, Deng J N, Zhang T 2016 *Acs Appl. Mater. Inter.* **8(10)** 6539
[23] Cui G, Zhang M, Zou G 2013 *Sci. Rep.* **3** 1250.
[24] Tang W, Wang J, Yao P J, Li X G 2014 *Sens. Actuators B* **192** 543
[25] Yong J K, Na H G, Kang S Y, Choi M S, Bang J H, Kim T W, Mirzaei A, Kim H W 2017 *Sens. Actuators B* **239** 180
[26] Huo L, Yang X, Liu Z, Tian X, Qi T, Wang X, Yu K, Sun J, Fan M 2017 *Sens. Actuators B* **244** 694
[27] Zhang M, Jiang G 2007 *Chinese Journal of Chemical Physics* **20** 315
[28] Wu R J, Wu J G, Yu M R, Tsai T K, Yeh C T 2008 *Sens. Actuators B* **131** 306
[29] Abe S, Choi U S, Shimanoe K, Yamazoe N 2005 *Sens. Actuators B* **107** 516
[30] Babaei M, Alizadeh N 2013 *Sens. Actuators B* **183** 617